Journal Pre-proof

MXenes as promising catalysts for water dissociation

José D. Gouveia, Ángel Morales-García, Francesc Viñes, Francesc Illas, José R.B. Gomes

Please cite this article as: Gouveia JD, Morales-García Á, Viñes F, Illas F, Gomes JRB, MXenes as promising catalysts for water dissociation, *Applied Catalysis B: Environmental* (2019), doi: https://doi.org/10.1016/j.apcatb.2019.118191

MXenes as promising catalysts for water dissociation

José D. Gouveia,[a] Ángel Morales-García,[b] Francesc Viñes,[b] Francesc Illas,[*b] José R. B. Gomes[*a]

[a]CICECO – Aveiro Institute of Materials, Department of Chemistry, University of Aveiro, Campus Universitário de Santiago, Aveiro, Portugal

[b]Departament de Ciència de Materials i Química Física & Institut de Química Teòrica i Computacional (IQTCUB), Universitat de Barcelona, c/Martí i Franquès 1-11, 08028 Barcelona, Spain

Corresponding authors: jrgomes@ua.pt; francesc.illas@ub.edu

Graphical Abstract

Break Water, My Friend

Research Highlights

- MXenes show great potential for catalyzing industrially relevant processes.
- MXenes (M = Ti, Zr, Hf, V, Nb, Ta, Cr, Mo; W; X = C; N) exothermically adsorb water.
- Activation energies for the first O-H bond cleavage in H2O are below 0.44 eV.
- MXenes dissociate water more effectively than surfaces containing noble metals.

Abstract

Two-dimensional few-layered transition-metal nitrides and carbides, called MXenes, have attracted a great interest given their large surface areas and their unique physicochemical properties. Motivated by the known reactivity of surfaces of bulk transition metal carbides on the mechanism behind the water-gas shift (WGS) reaction, density functional theory (DFT) calculations were employed to investigate the bonding of water and its dissociation on a set of eighteen M_2X MXene (M = Ti, Zr, Hf, V, Nb, Ta, Cr, Mo, and W, while X = C or N) surfaces. Here it is shown that all the studied MXenes exothermically adsorb water, with adsorption energies ranging from -1.43 to -2.94 eV, and greatly facilitate its dissociation, with energy barriers below 0.44 eV. These results reinforce the role of MXenes in promoting water dissociation, effectively suggesting their potential as catalysts for industrially relevant processes such as the WGS reaction.

Keywords: Water gas shift reaction; 2D materials; Carbides; Nitrides; Density functional theory; Periodic models;

1. Introduction

Understanding the molecular mechanism of water dissociative chemisorption as catalysed by different types of surfaces is extremely important, not only owing to its noted implications in a plethora of industrial processes, but also in many areas of fundamental research.[1] For instance, water dissociation often plays a determining role in the water-gas shift (WGS) reaction,[2-4] and it has also been suggested to promote CO oxidation and O_2 dissociation reactions catalysed by different surfaces.[5,6] Indeed, CeO_2-supported single-atoms (Au, Cu, and Pt)[3-6] and other systems have shown high catalytic performance towards the WGS reaction just because of their demonstrated potential to dissociate water. Also, computational studies suggest that dissociation of the first O–H bond of water is the rate-determining step (RDS) of the WGS reaction on copper surfaces,[7,8] although detailed kinetic Monte Carlo simulations show that, despite the water dissociation is an important step, the RDS may change depending on the reaction conditions[9] and the surface morphology.[10] Water dissociation is also relevant in the generation of hydrogen by means of the hydrogen evolution reaction (HER), where some two-dimensional metal-free based catalysts appear to be promising because of their large specific surface areas and, concomitantly, the high number of active sites per material gram.[11,12] Apart from the widely used supported catalysts consisting of metallic nanoparticles supported on porous oxides or sulphides,[13,14] and inspired by the landmark article by Levy and Boudard,[15] transition metal carbides (TMCs) have been gaining interest momentum as active phases[16] as well as supports for a diversity of catalysed reactions.[17] In particular for the WGS catalysed by the TiC(001) surface and TiC nanoparticles, it has been shown that the redox mechanism may become competitive with the associative one.[18]

The discovery of a new family of low-dimensional transition metal nitrides and carbides in 2011[19] provides a completely new scenario for such materials with unforeseen applications,[20] opening new possibilities for the use of carbides in catalysis. Inspired by the isolation of graphene,[21] these new two-dimensional (2D) materials were termed MXenes.[19] MXenes can be obtained by selective etching of the A element from a precursor MAX phase under a top-down synthesis procedure.[22-24] This MAX phase is described as an hexagonal layered ternary transition metal nitride or carbide, where M corresponds to an early transition metal (*e.g.* Ti, Zr, Hf, V, Nb, Ta, Cr, Mo, W), A stands for an element from a subset of groups XII-XVI, and X corresponds to either carbon (C) and/or nitrogen (N) elements.[25] The general formula of MXenes with $2n+1$ atomic layers is $M_{n+1}X_nT_x$, where M and X are the same as in the MAX phases, and T stands for the surface termination, usually determined by the synthesis conditions (*e.g.* -OH, -O, -H, or -F groups when using the hydrofluoric acid synthesis procedure).[19] Such layered MXenes display high electrical and metallic conductivity, hydrophilicity, large surface areas, tuneable structures, and a high oxidation resistance.[26-28] All of these properties, however, can suffer modifications upon hybridization with other materials and underpin the huge application potential of MXenes in areas such as ecofriendly energy generation,[29] water splitting and hydrogen generation,[30-32] and other heterogeneous catalysed reactions, such as dehydrogenation reactions.[33]

In addition, MXenes have also been explored in applications including energy storage[34-36] and gas sieving.[37-39]

The synthesis of bare MXenes is far from being straightforward and often results in functionalized MXenes exhibiting a mixture of terminations.[19,20] Notably, recent advances on HF-free syntheses have led to MXenes terminated by H and OH only.[40] Furthermore, post-synthesis heating treatments[41] were shown to allow defunctionalising the MXene surface and, very recently, were explored to improve the electronic conductivity displayed by these materials[42] The increase in the MXenes conductivity upon surface defunctionalisation is, in principle, beneficial for catalysis. In fact, there is recent experimental evidence that clean Ti_3C_2 is able to adsorb and activate CO_2,[43] confirming previous computational studies predicting that bare MXenes with M_2X stoichiometry have a high capacity for CO_2 abatement even at high temperature and low CO_2 partial pressures.[44,45] Since CO_2 is chemically inert, these results provide clear evidence that MXenes are very reactive for adsorbing and activating molecular species and pollutants.[46,47] The ability to produce MXenes exhibiting cleaned surfaces foresees a great potential in several chemical applications, from gas adsorption and separation,[48] to electrocatalysis,[49] heterogeneous catalysis[33], and photocatalysis.[50]

Motivated by earlier studies on the catalytic properties of bulk transition metal carbides,[16-18,51,52] here we investigate the possible application of MXenes as catalysts for the low temperature WGS reaction. To this end, we present a systematic study on the ability of a series of M_2X MXenes to catalyse the water O-H bond scission, regarded as the energetically most demanding step. Using electronic density-functional theory calculations and suitable models, we report and analyse the energy profiles for water dissociation, including energy barriers, thus shedding light on the underlying molecular mechanisms. The viability of MXenes as heterogeneous catalysts for water dissociation is discussed by making use of a detailed comparison to data reported in the literature for the same reaction on pure metal and metal alloy surfaces.

2. Models and methods

2.1. MXene models

A total of eighteen MXenes with M_2X stoichiometry (M = Ti, Zr, Hf, V, Nb, Ta, Cr, Mo, or W; and X = C or N) were selected to investigate the adsorption and dissociation of water, see Fig. 1. It is worth pointing out that the basal (0001) surface exhibited by the MXenes is equivalent to the (111) surface of bulk transition metal carbides (TMCs) with rocksalt structure. For these TMCs, the (111) surfaces have a considerable higher surface energy than the most stable (001) one.[53] Therefore, MXenes are predicted to be quite reactive and, on the other hand, allow one to investigate surfaces which could hardly exist otherwise in those bulk TMCs. To represent a situation with a small water coverage, each surface was modelled by a periodic $p(3\times3)$ supercell. Since a three-dimensional periodic symmetry is used for convenience, the dimension of the supercell in the direction perpendicular to the surface plane of the MXene was set to 16 Å. This ensures the presence of at least 10 Å of vacuum between periodic copies of the system, even after the adsorption of the H_2O molecule.

Table 1 compiles the calculated lattice parameter (a) of each studied MXene. MXenes composed of d^2 metals (Ti, Zr, and Hf) show the largest lattice parameters, followed by d^3 metals (V, Nb, and Ta), and d^4 ones (Cr, Mo, and W), regardless of whether they are N- or C-based. The calculated lattice parameters of Ti$_2$C (3.06 Å) and Ti$_2$N (2.98 Å) are in very good agreement with the respective values, 3.04 Å and 2.98 Å, found in the literature.[54] Finally, it is worth pointing out that these MXenes have been reported to be mechanically and dynamically stable.[55]

2.2. Computational details

The overall study relies on first-principles calculations carried out in the framework of density functional theory (DFT) using the Vienna *Ab initio* Simulation Package (VASP).[56] The calculations were carried out within the generalized gradient approximation (GGA) to the many-body exchange-correlation potential, namely using the functional introduced by Perdew, Burke, and Ernzerhof (PBE),[57] with the contribution of dispersion terms approximated through the D3 method as proposed by Grimme.[58] The valence electron density was expanded in a plane wave basis set with an energy cutoff of 415 eV. The effect of the atomic inner cores on the valence electron density was taken into account by means of the projector augmented wave (PAW) method.[59] The convergence criterion for the self-consistent field energies was set to 10^{-6} eV and structures were considered relaxed when the forces acting on all atoms were lower than 0.01 eV/Å. To carry out the necessary numerical integrations in the reciprocal space, the Brillouin zone was sampled using a Monkhorst-Pack 5×5×1 grid of special **k**-points.[60] Systematic convergence tests showed that, with this computational setup, calculations are converged within an accuracy of about 1 meV/atom. Spin polarisation was considered in all cases. This did not affect results on the M$_2$N systems but introduced some noticeable changes on a few M$_2$C MXenes, as discussed in more detail below.

For each species S, namely, H, OH, or H$_2$O, the adsorption energy (E_{ads}) is defined as

$$E_{ads} = E_{(S/MXene)} - (E_{MXene} + E_S) \tag{1},$$

where $E_{(S/MXene)}$, E_{MXene}, and E_S correspond to the total energy of the MXene containing the adsorbed species, the bare pristine MXene, and the isolated species, respectively. Note that the energies of the isolated H or OH species, E_S, were calculated as $E_H = {}^1/_2\, E_{H_2}$ and $E_{OH} = E_{H_2O} - \frac{1}{2}E_{H_2}$, respectively. The local minimum character of the ground state configurations was further characterized by calculating the normal modes of vibration of the adsorbed species and ensuring that all the eigenvalues of the dynamic matrix were positive, and, by that, that they correspond to real frequencies. The vibrational frequencies were obtained by diagonalization of the corresponding block of the Hessian matrix with elements computed as finite differences of 0.015 Å of analytical gradients. The calculated frequencies were also used to calculate the zero-point energy (ZPE) contribution to the total energy of both adsorbed and gas phase species. While the ZPE contributions

to the adsorption energies were all lower than 0.1 eV, they reduced some dissociation energy barriers by almost 0.2 eV.

The saddle point configuration for the minimum-energy pathway for H_2O dissociation on each MXene was located by using the dimer method.[61] The transition state (TS) structure characterized by the frequency analysis ensured a single imaginary frequency corresponding, precisely, to one O–H bond scission. This was verified by following bidirectionally the eigenvector of the dynamic matrix corresponding to the imaginary frequency, which yielded two minima adjacent to the saddle point consisting of a molecular and a dissociated adsorbed H_2O molecule. The dissociation energy barrier is defined as the amount of energy required to dissociate the adsorbed H_2O molecule into OH + H fragments, and is calculated, for each MXene, as the difference between the energy of the saddle-point configuration and that of the ground state adsorbed configuration of H_2O, both including the ZPE term.

3. Results and discussion

The dissociation of water on the explored MXene (0001) surfaces involves several steps, as depicted in Fig. 2. These are the adsorption of the water molecule onto the MXene surface, the dissociation of the water molecule into OH and H moieties, plus the eventual migration of OH and H fragments away from each other, *i.e.*, their diffusion on the surface towards their respective most stable adsorbed sites. In this study, we mainly focus on the first two steps. To simplify the discussion of our results, the results for H, OH, and H_2O adsorption on MXene surfaces are separated from those corresponding to the dissociation step.

3.1. Adsorption of H, OH, and H_2O on MXene surfaces

The study of H adsorption constitutes the simplest to analyse, as the most favourable adsorption site of the H atom is over the centre of an H_M site, see Fig. 1, around 1 Å above the plane of the MXene surface regardless of the type of MXene substrate. The calculated adsorption energies are all negative, see Table 1, indicating that the H atom adsorption is energetically favourable. The adsorption energies of H on Cr_2C and Zr_2C surfaces were the only ones affected by the inclusion of the spin polarisation: The H adsorption energy on Cr_2C became 0.11 eV lower whereas that on Zr_2C became 0.11 eV larger. The calculated results indicate that the adsorption is stronger on MXenes composed of d^2 metals (Ti, Zr, and Hf) and becomes weaker for d^3 and d^4 metals. Both nitride and carbide MXenes have H adsorption energies in the same range.

The most stable state adsorption sites for the OH species and their respective adsorption energies on the MXene surfaces are compiled in Table 3. The adsorption occurs systematically with the O atom closer to the surface and with the OH bond perpendicular to it. However, unlike the case of the H adatom, the OH adsorption site depends on the MXene. For both d^2 and d^3 MXenes, the OH moiety interacts perpendicularly to the surface with the O atom about 1.3 Å away from the plane of the surface and on an H_M site. On the other hand, on Cr_2C, Mo_2C, and Mo_2N surfaces, the adsorption on H_X and H_M sites is competitive within 0.1 eV.

Additionally, on Cr_2N and W_2C surfaces, OH prefers H_N and H_C sites, respectively. Finally, on W_2N, OH adsorbs on top of a metal atom, which interacts with the O atom of the molecule. On this MXene, the O atom of OH is located about 1.9 Å away from the nearest W atom, in a configuration with C_1 symmetry. Indeed the adsorption of OH on the W_2N surface involves a distortion of the neighbouring lattice, characterized especially by the nearest W atom moving more than 1 Å away from the MXene plane. In general, the OH adsorption energy ranges from -1.5 to almost -3.0 eV, showing that the process is energetically favourable. Spin polarisation affects the adsorption of OH on Ti_2C and Cr_2C surfaces, causing it to become 0.16 eV weaker and stronger, respectively, Table 3. The absolute value of the adsorption energy is larger on d^2 MXenes (Ti, Zr, and Hf) and becomes smaller for d^3 and d^4 MXenes, with the sole exception of W_2N.

Depending on the MXene surface, the adsorption of the H_2O molecule takes place on either bridge (B) or top (T) sites, see Fig. 3. In the former, the oxygen atom of the water molecule is located on a B site, between two metal atoms of the MXene surface, and each hydrogen atom lies above sites labelled as H_M/H_X that are adjacent to the B site binding the water molecule. On B sites, the distance between the O atom and the surface plane is around 1.8 Å. On the T configuration, the oxygen atom is above a top site of the MXene surface and each hydrogen is above a nearby H_M site. The distance between the O atom and the surface plane is about 2.2 Å.

The energy differences between the two most stable configurations are small, between 0.2 and 0.4 eV. Table 4 compiles the H_2O adsorption energy along with the corresponding site. Our results indicate that d^3 and d^4 MXenes adsorb water preferably on the T configuration, whereas d^2 MXenes can adsorb on either T or B. In particular, the adsorption of water on a B site is the most stable for Ti_2N, Zr_2C, and Hf_2C, whereas the T configuration is the most stable in Ti_2C and Hf_2N. Finally, for Zr_2N, the adsorption sites are competitive within $\Delta E_{ads} < 0.1$ eV. The adsorption energy ranges from -0.8 to -1.1 eV on both C- and N-based MXenes, with slightly higher absolute values corresponding to MXenes on which H_2O adsorbs at the bridge configuration. In the case of water adsorption, spin polarisation only affects Ti_2C, where the adsorption becomes stronger by 0.24 eV when including spin polarisation and the ground state configuration changes from B to T. Curiously, without spin polarisation, the T structure is not even metastable for Ti_2C and its energy could only be evaluated by imposing symmetry restrictions.

It is interesting to compare the present results for the MXenes with those in a very recent computational work concerning the H_2O adsorption on the (111) surfaces of TiC, VC, ZrC, and NbC.[62] In that work, it was predicted that water adsorption would occur preferably on an H_C site. We tested this possibility, along with the adsorption on an H_M site, but both were found unstable for all MXenes and, after geometry optimization, the molecule relaxed to either the T- or B-adsorbed structures. This shows that the adsorption configuration can change not only by switching the X atom but also by changing the number of atomic layers and/or the stoichiometry, which can affect concomitantly the electronic structure. Nevertheless, weak bonding with adsorption energies just below 1 eV are a common feature between both types of systems.

3.2. Dissociation of H_2O on MXene surfaces

In the quest of using the dimer method to search for transition states, two different types of saddle-point structures were located, depending on the molecular water adsorption site, see Fig. 3. Please note that in Fig. 3, the top row panels are representative of water dissociation reactions on MXene surfaces where the adsorbate is preferentially located at the B site, whereas the bottom row panels are representative of MXene surfaces preferentially adsorbing water at the T sites. The dissociative mechanism of water initially adsorbed on a B site, found in Ti_2N, Zr_2C, and Hf_2C MXenes, involves a rotation of the H_2O molecule by about 15° around the axis perpendicular to the molecular plane, followed by a displacement of the whole molecule towards the nearby H_M site. The resemblance between the ground state and the transition state is reflected in dissociation energy barriers (E_{diss}) lower than 0.1 eV (see Table 5), practically unaffected by the ZPE term. On the other hand, the dissociation mechanism for surfaces where H_2O is initially adsorbed at the T site involves one of the H atoms of water being pulled away from the O atom and being drawn closer to the surface, towards a nearby H_M site, which, indeed, is the corresponding preferred adsorption site for atomic H. The dihedral angle between the molecular and surface planes is around 40°. For the MXenes where water adsorbs at the T site, the dissociation energy barriers are larger than the ones corresponding to the B sites (with the exception of Hf_2N) and up to 0.44 eV (see Table 5). Here the ZPE term on E_{diss} decreases the barriers by 0.17-0.19 eV.

Hence, the main difference between the two dissociative mechanisms is the orientation of H_2O with respect to the (0001) MXene surface. As clearly seen in Fig. 3, when the molecule is adsorbed at a B site, the H_2O molecular plane is perpendicular to the surface, whereas for the adsorption on a T site both planes are almost parallel. In general, dissociation of molecules siting at the T site requires larger energy barriers. For this reason, in the cases where H_2O is preferentially adsorbed at a T site, the molecule could migrate to (or close to) a B site and then dissociate almost spontaneously. To test this hypothesis, we calculated the dissociation energies of water at the B configuration on the MXene surfaces where the most stable adsorption occurs on a T site. In all cases, the calculated energy barriers were of at least 0.2 eV, which is in clear contrast with the values below 0.1 eV found for the corresponding MXenes where H_2O is preferentially adsorbed at B sites. Therefore, the hypothesis of migration from B to T was ultimately discarded since the migration energy from T to B, added to the dissociation energy on site B, exceeds the dissociation energy on site T by at least 0.1 eV, and by that implying that migration to B site followed by dissociation is a less likely process. Nonetheless, the transition state shown in the bottom images of Fig. 3 corresponding to the MXenes where H_2O adsorbs at site T, features an intermediate structure between configurations for H_2O adsorption at the T and B sites. Finally, the E_{diss} values compiled in Table 5 show that the d^2 MXenes exhibit the smallest energy barriers followed by the d^3 and d^4 MXenes. In general, the dissociation of water is energetically slightly easier in carbide MXenes than in their nitride counterparts. Regardless of the mechanism, the dissociation energy

barriers range from 0.05 to 0.44 eV, and so, are minimal, highlighting the great H_2O breaking power of MXenes.

After H_2O dissociation, the products of the reaction are not necessarily located at their most stable sites. Indeed, the absolute values of the $E_{reaction}$ in Table 5 are larger when the dissociation products end up farther from each other. Nevertheless, in all cases water dissociation is thermodynamically favoured. The energy difference between $E_{ads}(OH) + E_{ads}(H)$ and $E_{ads}(H_2O) + E_{reaction}$, labelled as ΔE_∞, see Fig. 2, stands for the amount of energy that the system can still gain after the dissociation of H_2O into OH and H when moving the two product species farther apart from each other into their own ground state adsorption sites. Defined like this, a value of ΔE_∞ close to zero represents an OH+H configuration that is already stable immediately after dissociation. Contrarily, values of ΔE_∞ much smaller than zero can be visually confirmed to be associated with configurations after the dissociation of H_2O, in which the OH and H moieties are still too close to each other and not on their most favourable adsorbed sites. Fig. 4a presents a plot of activation energies (E_{diss}) *versus* the full reaction energy ($E_{reaction} + \Delta E_\infty$); the rather good linear correlation implies that a Brønsted-Evans-Polanyi (BEP) relationship holds,[63-65] which may be useful to explore trends in other MXenes. In addition, Fig. 4b shows a second plot corresponding to activation energies (E_{diss}) *versus* the d-band centre (ε_d),[66,67] obtained from the d projection of the density of states (DOS) of one surface metal atom, following a procedure established in the literature.[68,69] The MXenes featuring high E_{diss} values have low ε_d, in contrast with the larger ε_d found where the E_{diss} are low, as expected. According to the linear correlations of Fig. 4, low activation energies (E_{diss}) are accompanied by highly negative reaction energies ($E_{reaction} + \Delta E_\infty$) and high ε_d values. In general, the predicted energy barriers are all below 0.5 eV indicating that MXenes, especially the d^2 ones, are highly active for water dissociation.

Finally, it is worth comparing the present results for H_2O dissociation on MXenes with other employed materials, even if a rigorous comparison is not possible because different calculation parameters are often used, a qualitative comparison is viable. On Pt surfaces, H_2O adsorption energies, predicted without accounting for dispersion terms, vary between -0.27 and -0.69 eV, depending on the considered surface plane.[70] There water adsorbs on a top position, and the distances between the O atom and the nearest Pt atom are in the 2.2–2.5 Å range. Comparing with the present results, one can conclude that water adsorbs more strongly on MXenes than on Pt and, as well as closer to the surface. For the present set of MXenes, the largest activation energy for water dissociation is 0.44 eV, almost coinciding with the lowest one found in low Miller index Pt surfaces,[70] thus unfolding that MXenes are more efficient catalysts than Pt for water dissociation. These findings also reinforce the common assumption that TMCs are catalysts similar, or even better, than Pt-group metals.[15] Note also that the dissociation reaction was predicted to be endothermic on three of the five Pt surfaces studied,[70] while here it is clearly exothermic in all the investigated MXenes. The molecular dissociation mechanism is also similar to that reported for a Pt_{79} nanoparticle, for a Pt_8 cluster in gas phase, this Pt_8 deposited on a $CeO_2(111)$ surface, and also for a $Ce_{40}O_{80}$ nanoparticle.[4] For these systems, the water

adsorption energies range between -0.5 and -1.0 eV, a similar order of magnitude as the one found for the MXene surfaces, see Table 4. However, the corresponding energy barriers are in the 0.5–0.7 eV range,[4] thus significantly larger than the barriers predicted here for the scrutinized MXene surfaces, see Table 5. Finally, note that water dissociation on a TiC(001) extended surface implies an energy barrier of 0.37 eV,[18] quite low, but still larger than the barrier reported for the MXene surfaces.

Boumaza et al. reported that the ternary catalyst based on the $Cu_{0.5}Zn_{0.5}Al_2O_4$ spinel oxide shows high activity for the WGS reaction at low temperature.[71] A recent computational study compared the activities displayed by different ternary catalysts models and showed that Cu surfaces doped with Zn and Al atoms were quite active in the dissociation of the H_2O molecule into OH and H species.[72] The energy barriers, incorporating zero-point energy corrections, are in the range between 0.21 eV and 0.44 eV, being the most active the $(AlZn)_tCu(100)$ model, i.e., a Cu(100) surface with two Cu atoms in the exposed surface replaced by one Al and one Zn. The water dissociation reactions were exothermic by -0.41 eV to -0.98 eV. The Cu/Zn/Al ternary catalysts are more active in dissociating H_2O than catalysts based on Cu/Pt/Ru, Cu/Rh/Ru and Cu/Ni/Ru combinations. Thus, while the calculations confirm the experimental evidences that catalysts derived from Cu/Zn/Al combinations of metals are interesting for the WGS reaction, it arises from the results in the present work that MXenes may have the potential for being considered as promising materials for water dissociation.

It is pertinent to point out that, in practice, the WGS reaction requires temperatures of a few hundred Celsius. On the other hand, it has been shown that the Ti_3C_2 MXene is stable up to 800 °C in Ar atmosphere[73] and that high temperatures contribute to maintain some regions of the MXene surfaces clean enough.[41] Hence, the MXenes are expected to be stable (and very active) at the temperatures required for the WGS reaction. It is worth mentioning here that, if the MXene surface is fully terminated, the catalyst loses its outstanding reactivity and molecules adsorb less exothermically. Nevertheless, preliminary calculations with oxygen-terminated MXenes show that the dissociation reactions are practically unaffected provided the O coverage is below 66 %. Let us now consider the subsequent steps of the WGS reaction taking the Ti_2C catalyst surface as an example. It is well known that OH-terminated MXenes are quite stable, and the terminating OH groups are almost not reactive. The results from the preliminary DFT calculations also revealed an activation energy for OH dissociation into O+H of 0.53 eV (expectedly, this is higher than the first O-H bond scission requiring 0.09 eV only) and a reaction energy of -1.87 eV. The adsorption of CO is highly exothermic (-3.05 eV) and the formation of H_2 (with spontaneous desorption after formation) and CO_2 are both endothermic, with reaction energies of +2.71 eV and +2.41 eV. Overall, the whole WGS reaction on Ti_2C is exothermic by -3.96 eV. Therefore, under operating conditions, MXenes are expected to be active catalysts for the WGS reaction although, obviously, this prediction requires further confirmation from additional theoretical studies and, eventually, from appropriate experiments.

4. Conclusions

The adsorption and dissociation of water on eighteen MXenes (0001) surfaces with M_2X (M = Ti, Zr, Hf, V, Nb, Ta, Cr, Mo, or W; and X = C or N) stoichiometry have been investigated by using first-principles DFT based calculations, including the approximate contribution of dispersion. The calculated results show that the water molecular adsorption is an exothermic process on all the analysed MXenes. Depending on the considered surface, the water molecule adsorbs either on a bridge or a top position. Ti_2N and Zr_2C emerge as the most reactive substrates of all nitrides or carbides, respectively. No trend was observed between H_2O adsorption energies along periods or groups, or with the distance between the adsorbed molecule and the surface. In all cases, H_2O dissociation on MXenes is exothermic with absolute reaction energies higher than 1 eV on most MXenes, up to 3.35 eV for Hf_2N. Different transition state configurations were found depending on the preferential bridge or top H_2O adsorption site. In all MXenes, the reaction activation energy barriers were found to be relatively small, *i.e.*, below 0.44 eV. Barriers tend to be slightly larger for nitride MXenes than for the corresponding carbide counterparts, and to increase along the periodic table periods. The MXenes which adsorb water into a bridge configuration (Zr_2C, Hf_2C, and Ti_2N) display very small dissociation energy barriers, below 0.1 eV. Finally, the reaction energy and the *d*-band centre constitute good descriptors that may be used to efficiently screen the capability of other MXenes for water dissociation. Overall, the present results reinforce the view of MXenes as active catalysts for water dissociation.

Conflicts of interest

There are no conflicts to declare

Acknowledgements

Table 1 Calculated lattice parameter (*a*) of carbide (M_2C) and nitride (M_2N) MXenes. All values are given in Å.

a	M	M_2C	M_2N
d^2	Ti	3.06	2.98
	Zr	3.27	3.24
	Hf	3.21	3.17
d^3	V	2.90	2.89
	Nb	3.13	3.15
	Ta	3.09	3.09
d^4	Cr	2.82	2.68
	Mo	3.10	2.79
	W	2.88	2.78

Table 2 Adsorption energies of a single H adatom on the MXene (0001) surfaces. Notice that the adsorption site is H_M for all cases. The reference for the H species in the gas phase has been taken as half the energy of a hydrogen molecule, $E_H = {}^{1}/_{2} E_{H_2}$. All values are given in eV.

E_{ads}^{H}	M	M_2C	M_2N
d^2	Ti	-1.35	-1.44
	Zr	-1.18	-1.39
	Hf	-1.34	-1.39
d^3	V	-1.24	-1.04
	Nb	-1.19	-1.04
	Ta	-1.19	-0.97
d^4	Cr	-1.07	-0.89
	Mo	-0.86	-0.98
	W	-0.87	-0.87

Table 3 Adsorption sites and energies of OH species on the MXene (0001) surfaces. Labelling for adsorption sites as in Figure 1 and bold highlights the most stable site in cases of degenerate structures. The reference energy for the OH species in the gaseous phase has been chosen as $E_{OH} = E_{H_2O} - \frac{1}{2}E_{H_2}$. All values are given in eV.

E_{ads}^{OH}	M	M_2C		M_2N	
d^2	Ti	H_M	-2.80	H_M	-2.93
	Zr	H_M	-2.81	H_M	-2.81
	Hf	H_M	-2.94	H_M	-2.86
d^3	V	H_M	-2.38	H_M	-2.08
	Nb	H_M	-2.24	H_M	-2.01
	Ta	H_M	-2.20	H_M	-1.93
d^4	Cr	H_C/**H_M**	-2.08	H_N	-1.96
	Mo	**H_C**/H_M	-1.58	**H_N**/H_M	-1.43
	W	H_C	-1.48	T	-2.26

Table 4 Adsorption sites and energies of the water molecule on the MXene (0001) surfaces. For Zr_2N, competing configurations are found, B being the most stable one. All values are given in eV.

$E_{ads}^{H_2O}$	M	M_2C		M_2N	
d^2	Ti	T	-0.85	B	-1.05
	Zr	B	-0.97	**B**/T	-0.86
	Hf	B	-0.93	T	-0.89
d^3	V	T	-0.88	T	-0.87
	Nb	T	-0.83	T	-0.83
	Ta	T	-0.88	T	-0.90
d^4	Cr	T	-0.93	T	-0.77
	Mo	T	-0.92	T	-0.81
	W	T	-0.79	T	-0.86

**Table 5** Dissociation energy barrier, E_{diss}, reaction energy, $E_{reaction}$, and energy contribution due to reactants separation, ΔE_∞, for water dissociation on the MXene (0001) surfaces. Definitions are as in the caption of Fig. 2, and all values are given in eV.

	M	M_2C			M_2N		
		E_{diss}	$E_{reaction}$	ΔE_∞	E_{diss}	$E_{reaction}$	ΔE_∞
d^2	Ti	0.09	-3.30	0.00	0.07	-3.29	-0.03
	Zr	0.06	-2.51	-0.51	0.07	-3.32	-0.02
	Hf	0.05	-2.69	-0.67	0.05	-3.35	-0.01
d^3	V	0.14	-2.70	-0.04	0.25	-2.20	-0.05
	Nb	0.17	-2.58	-0.02	0.22	-1.89	-0.33
	Ta	0.16	-1.29	-1.22	0.38	-1.27	-0.73
d^4	Cr	0.31	-1.97	-0.62	0.39	-1.70	-0.01
	Mo	0.33	-0.99	-0.53	0.39	-1.58	-0.01
	W	0.44	-0.44	-1.12	0.40	-2.22	-0.05

17

Fig. 1 Top view of the $p(3\times3)$ supercell employed to model the MXene (0001) surfaces. The top and bottom layers (light blue spheres) are made up of atoms of a transition metal (M), while the central layer (X) consists of carbon or nitrogen atoms (navy spheres). The rhombus represents the boundaries of the used cell. Letters inside the gray spheres indicate the labelling for the four relevant high-symmetry sites on the catalyst surface: bridge (B), top (T), hollow metal (H_M), and hollow carbon/nitrogen (H_X, in practice, H_C or H_N).
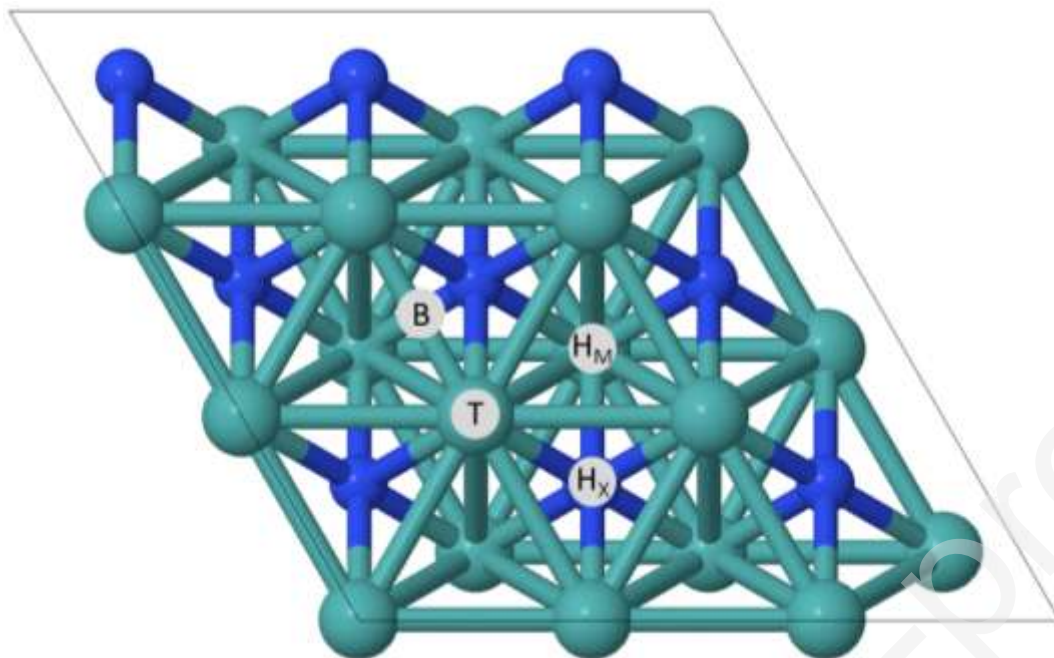
**Fig. 2** Schematic energy profile for the water dissociation on MXenes. Step *i)* corresponds to molecular adsorption $E_{ads}^{H_2O}$, *ii)* to dissociation into coadsorbed OH+H, E_{diss}, and *iii)* to separation of the reaction products to their most stable adsorbed sites, ΔE_∞. The value of $E_{ads}^{OH} + E_{ads}^{H}$ is the sum of the adsorption energies of OH and H on the MXene.
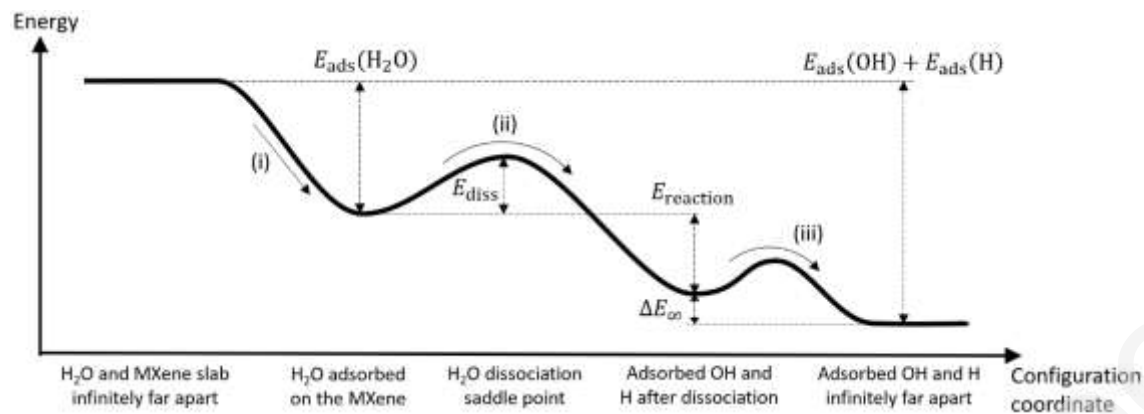
Fig. 3 Top and side views of the molecular, transition and dissociated states for the water dissociation reaction on bridge sites of the Zr_2C surface (first row panels) and on top sites of the Mo_2N surface (second row panels). Colour code: oxygen is red; hydrogen is white; carbon is grey; nitrogen is navy blue; zirconium is teal; and molybdenum is green.
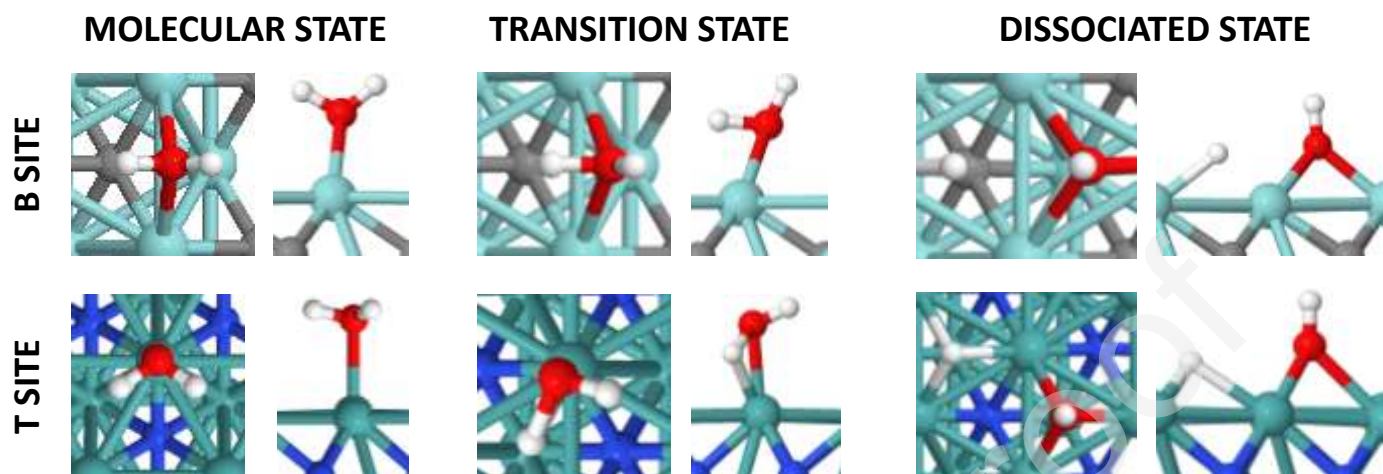
Fig. 4 (a) Plot of the Brønsted–Evans–Polanyi (BEP) relationship for the water dissociation reaction on the MXene surfaces investigated; the black solid line was obtained by linear regression and has the equation $E_{\text{diss}} = 0.195 \cdot (E_{\text{reaction}} + E_\infty) + 0.711$, with a correlation coefficient $R = 0.916$. (b) Correlation between E_{diss} and the d-band centre, ε_d; the black solid line was obtained by linear regression and has the equation $E_{\text{diss}} = -0.067 \cdot \varepsilon_d + 0.321$, with a correlation coefficient $R = 0.835$. Red and blue dots correspond to carbide and nitride MXenes, respectively.
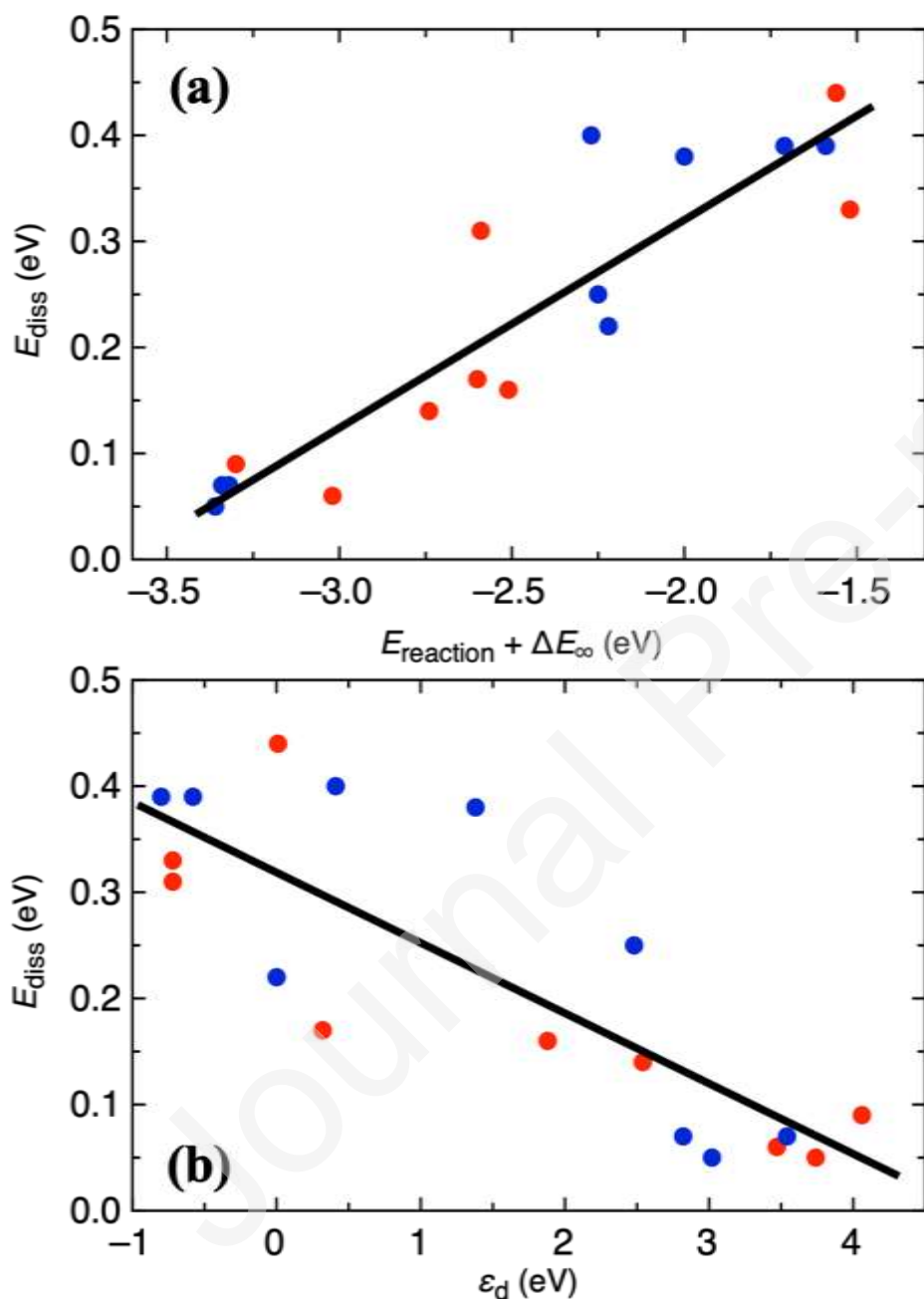
References

(1) A. Hodgson and S. Haq, *Surf. Sci. Rep.*, 64 (2009) 381-451.

(2) Z. P. Liu, S. J. Jenkins and D. A. King, *Phys. Rev. Lett.*, 94 (2005) 196102.

(3) J. A. Rodríguez, P. Liu, J. Hrbek, J. Evans and M. Pérez, *Angew. Chem. Int. Ed.*, 46 (2007) 1329-1332.

(4) A. Bruix, J. A Rodríguez, P. J. Ramírez, S. D. Senanayake, J. Evans, J. B. Park, D. Stacchiola, P. Liu, J. Hrbek and F. Illas, *J. Am. Chem. Soc.*, 134 (2012) 8968-8974.

(5) Y. Gao and X. C. Zeng, *ACS Catal.*, 2 (2012) 2614-2621.

(6) J. Saavedra, H. A. Doan, C. J. Pursell, L. C. Grabow, B. D. Chandler, *Science*, 345 (2014) 1599-1602.

(7) J. L. C. Fajin, M N. D. S. Cordeiro, F. Illas and J. R. B. Gomes, *J. Catal.*, 268 (2009) 131-141.

(8) A. Gokhale, J. A. Dumesic and M. Mavrikakis, *J. Am. Chem. Soc.*, 130 (2008) 1402-1414.

(9) H. Prats, L. Álvarez-Falcón, F. Illas and R. Sayós, *J. Catal.*, 333 (2016) 217-226.

(10) H. Prats, P. Gamallo, F. Illas and R. Sayós, *J. Catal.*, 342 (2016) 75-83.

(11) K. K. Ghuman, S. Yadav and C. V. Singh, *J. Phys. Chem. C*, 119 (2015) 6518-6529.

(12) N. Q. Tran, V. Q. Bui, H. M. Le, Y. Kawazoe and H. Lee, *Adv. Energy Mater.*, 8 (2018) 1702139.

(13) B. C. Gates, *Chem. Rev.*95 (1995) 511-522.

(14) A. Corma and H. Garcia, *Chem. Rev. Soc.*, 37 (2008) 2096-2126.

(15) R. B. Levy and M. Boudard, *Science*, 181 (1973) 547-549.

(16) H. H. Hwu and J. G. Chen, *Chem. Rev.* 105 (2005) 185-212.

(17) J. A. Rodriguez and F. Illas, *Phys. Chem. Chem. Phys.* 14 (2012) 427-438.

(18) F. Viñes, J.A. Rodriguez, P. Liu and F. Illas, *J. Catal.*, *260* (2008) 103-112.

(19) M. Naguib, M. Kurtoglu, V. Presser, J. Lu, J. Niu, M. Heon, L. Hultman, Y. Gogotsi and M. W. Barsoum, *Adv. Mater.*, 23 (2011) 4248–4253.

(20) M. Naguib and Y. Gogotsi, *Acc. Chem. Res.*, 48 (2015) 128-135.

(21) K. S. Novoselov, A. K. Geim, S. V. Morozov, D. Jiang, M. I. Katsnelson, I. V. Grigorieva, S. V. Dubonos and A. A. Firsov, *Nature*, 438 (2005) 197–200.

(22) M. Alhabeb, K. Maleski, T. S. Mathis, A. Sarycheva, C. B. Hatter, S. Uzun, A. Levitt and Y. Gogotsi, *Angew. Chem. Int. Ed.*, 57 (2018) 5444-5448.

(23) M. Alhabeb, K. Maleski, B. Anasori, P. Lelyukh, L. Clark, S. Sin and Y. Gogotsi, *Chem. Mater.*, 29 (2017) 7633-7644.

(24) O. Mashtalir, M. Naguib, V. N. Mochalin, Y. Dall´Agnese, M. Heon, M. W. Barsoum and Y. Gogotsi, *Nat. Commun.*, 4 (2013) 1716.

(25) J. Peng, X. Chen, W. J. Ong, X. Zhao and N. Li, *Chem*, 5 (2019) 18–50.

(26) H. Wang, Y. Wu, X. Yuan, G. Zeng, J. Zhou, X. Wanga and J. W. Chew, *Adv. Mater.*, 30 (2018) 1704561.

(27) Q. Jiang, N. Kurra, M. Alhabeb, Y. Gogotsi and H. N. Alshareef, *Adv. Energy Mater.*, 8 (2018) 1703043.

(28) B. Anasori, M. R. Lukatskaya and Y. Gogotsi, *Nat. Rev. Mater.*, 2 (2017) 16098.

(29) L. Zhao, B. Dong, S. Li, L. Zhou, L. Lai, Z. Wang, S. Zhao, M. Han, K. Gao, M. Lu, X. Xie, B. Chen, Z. Liu, X. Wang, H. Zhang, H. Li, J. Liu, H. Zhang, X. Huang and W. Huang, *ACS Nano*, 11 (2017) 5800-5807.

(30) C. Lu, D. Tranca, J. Zhang, F. Rodríguez Hernández, Y. Su, X. Zhuang, F. Zhang, G. Seifert and X. Feng, *ACS Nano*, 11 (2017) 3933-3942.

(31) G. Gao, A. P. O'Mullane and A. Du, *ACS Catal.*, 7 (2017) 494-500.

(32) L. Ma, L. R. L. Ting, V. Molinari, C. Giordano and B. S. Yeo, *J. Mater. Chem. A*, 3 (2015) 8361-8368.

(33) J. Y. Diao, M. M. Hu, Z. Lian, Z. J. Li, H. Zhang, F. Huang, B. Li, X. H. Wang, D. S. Su, H. Y. Liu, *ACS Catal.*, 8 (2018) 10051-10057.

(34) M.-S. Cao, Y.-Z. Cai, J.-C. Cai, P. He, J. C. Shu, W. Q. Cao and J. Yuan, *Chem. Eng. J.*, 359 (2019) 1265-1302.

(35) C. Couly, M. Alhabeb, K. L. Van Aken, N. Kurra, L. Gomes, A. M. Navarro-Suárez, B. Anasori, H. N. Alshareef and Y. Gogotsi. *Adv. Electron. Mater.*, 4 (2018) 1700339.

(36) M. R. Lukatskaya, S. Kota, Z. Lin, M.-Q. Zhao, N. Shpigel, M. D. Levi, J. Halim, P.-L. Taberna, M. W. Barsoum, P. Simon and Y. Gogotsi. *Nat. Energy*, 2 (2017) 17105.

(37) L. Ding, Y. Wei, L. Li, T. Zhang, H. Wang, J. Xue, L.-X. Ding, S. Wang, J. Caro and Y. Gogotsi, *Nat. Commun.*, 9 (2018) 155.

(38) J. Shen, G. Liu, Y. Ji, Q. Liu, L. Cheng, K. Guan, M. Zhang, G. Liu, J. Xiong, J. Yang and W. Jin, *Adv. Funct. Mater.*, 2018, 28, 1801511.

(39) L. Li, T. Zhang, Y. Duan, Y. Wei, C. Dong, L. Ding, Z. Qiao and H. Wang, *J. Mater. Chem. A*, 6 (2018) 11734-11742.

(40) T. Li, L. Yao, Q. Liu, J. Gu, R. Luo, J. Li, X. Yan, W. Wang, P. Liu, B. Chen, W. Zhang, W. Abbas, R. Naz and D. Zhang, *Angew. Chem. Intl. Ed.*, 57 (2018) 6115–6119.

(41) E. B. Deeva, A. Kurlov, P. M. Abdala, D. Lebedev, S. M. Kim, C. P. Gordon, A. Tsoukalou, A. Fedorov and C. R. Müller, *Chem. Mater.*, 31 (2019) 4505-4513.

(42) J. L. Hart, K. Hantanasirisakul, A. C. Lang, B. Anasori, D. Pinto, Y. Pivak, J. Tijn van Omme, S. J. May, Y. Gogotsi and M. L. Taheri, *Nat. Comm.* 10 (2019) 522.

(43) I. Persson, J. Halim, H. Lind, T. W. Hansen, J. B. Wagner, L.-Å. Näslund, V. Darakchieva, J. Palisaitis, J. Rosen and P. O. Å Persson, *Adv. Mater.* 31 (2019) 1805472.

(44) Á. Morales-García, A. Fernández-Fernández, F. Viñes and F. Illas, *J. Mater. Chem. A*, 6 (2018) 3381-3385.

(45) R. Morales-Salvador, Á. Morales-García, F. Viñes and F. Illas, *Phys. Chem. Chem. Phys.*, 20 (2018) 17117-17124.

(46) X. Yu, Y. Li, J. Cheng, Z. Liu, Q. Li, W. Li, X. Yang and B. Xiao, *ACS Appl. Mater. Interfaces*, 7 (2015) 13707-13713.

(47) Y. Zhang, L. Wang, N. Zhang and Z. Zhou, *RSC Adv.*, 8 (2018) 19895-19905.

(48) A. Junkaew and R. Arroyaveb, *Phys. Chem. Chem. Phys.,* 20 (2018) 6073-6082.

(49) Z. Wei Seh, K. D. Fredrickson, B. Anasori, J. Kibsgaard, A. L. Strickler, M. R. Lukatskaya and Y. Gogotsi, T. F. Jaramillo, A. Vojvodic, *ACS Energy Lett.*, 1 (2016) 589-594.

(50) Z. Guo, J. Zhou, L. Zhua and Z. Sun, *J. Mater. Chem. A*, 4 (2016) 11446-11452.

(51) X. Liu, C. Kunkel, P. Ramírez de la Piscina, N. Homs, F. Viñes and F. Illas, *ACS Catal.*, 7 (2017) 4323-4335

(52) S. Posada-Pérez, P. Ramírez, R. Gutiérrez, D. Stacchiola, F. Viñes, P. Liu, F. Illas and J. A. Rodriguez, *Catal. Sci. Technol.*, 6 (2016) 6766-6777.

(53) A. Vojvodic, C. Ruperto and B. I. Lundqvist, *J. Phys.: Condens. Matter*, 22 (2010) 375504.

(54) N. Zhang, Y. Hong, S. Yazdanparast and M. A. Zaeem, *2D Mater.*, 5 (2018) 045004.

(55) U. Yorulmaz, A. Özden, N. H. Perkgöz, F. Ay and C. Sevik, *Nanotechnology*, 27 (2016) 335702.

(56) G. Kresse and J. Furthmüller, *Phys. Rev. B*, 54 (1996) 11169.

(57) J. P. Perdew, K. Burke and M. Ernzerhof, *Phys. Rev. Lett.*, 77 (1996) 3865-3868.

(58) S. Grimme, J. Antony, S. Ehrlich and H. Krieg, *J. Chem. Phys.*, 132 (2010) 154104.

(59) P. E. Blöchl, *Phys. Rev. B*, 50 (1994) 17953.

(60) H. J. Monkhorst and J. D. Pack, *Phys. Rev. B*, 13 (1976) 5188.

(61) G. Henkelman and H. Jónsson, *J. Chem. Phys.*, 111 (1999) 7010.

(62) F. Silveri, M. G. Quesne, A. Roldan, N. H. De Leeuw and C. R. A. Catlow, *Phys. Chem. Chem. Phys.*, 21 (2019) 5335-5343.

(63) M. G. Evans and M. Polanyi, *Trans. Faraday Soc.*, 34 (1938) 11-24.

(64) J. N. Brønsted, *Chem. Rev.*, 5 (1928) 231-338.

(65) R. P. Bell, *Proc. R. Soc. London, Ser. A*, 154 (1936) 414-429.

(66) B. Hammer and J. K. Nørskov, *Surf. Sci.,* 343 (1995) 211-220.

(67) B. Hammer and J. K. Nørskov, *Nature*, 376 (1995) 238-240.

(68) V. Pallassana and M. Neurock, *J. Catal.*, 191 (2000) 301–317.

(69) J. L. C. Fajín, A. Bruix, M. N. D. S. Cordeiro, J. R. B. Gomes and F. Illas, *J. Chem. Phys.*, 137 (2012) 034701.

(70) J. L. C. Fajín, M. N. D. S. Cordeiro and J. R. B. Gomes, *J. Phys. Chem. A*, 118 (2014) 5832-5840.

(71) S. Boumaza, A. Auroux, S. Bennici, A. Boudjemaa, M. Trari, A. Bouguelia and R. Bouarab, *Reac. Kinet. Mech. Cat.,* 100 (2010) 145–151.

(72) J. L. C. Fajín, M. N. D. S. Cordeiro and J. R. B. Gomes, *Appl. Catal. B: Environmental*, 218 (2017) 199-207.

(73) Z. Li, L. Wang, D. Sun, Y. Zhang, B. Liu, Q. Hu, A. Zhou, *Mat. Sci. and Eng.: B*, 191 (2015) 33-40.